metals

MDPI

Article

New Insight on the Hydrogen Absorption Evolution of the Mg–Fe–H System under Equilibrium Conditions

Julián Puszkiel [1,2,*], M. Victoria Castro Riglos [3], José M. Ramallo-López [4], Martin Mizrahi [4], Thomas Gemming [5], Claudio Pistidda [2], Pierre Arneodo Larochette [1], José Bellosta von Colbe [2], Thomas Klassen [2,6], Martin Dornheim [2] and Fabiana Gennari [1]

1 Department of Physical Chemistry of Materials, Consejo Nacional de Investigaciones Científicas y Técnicas (CONICET) and Centro Atómico Bariloche, Av. Bustillo km 9500, San Carlos de Bariloche P.C. 8400, Argentina; arneodo@gmail.com (P.A.L.); gennari@cab.cnea.gov.ar (F.G.)
2 Department of Nanotechnology, Institute of Materials Research, Helmholtz–Zentrum Geesthacht, Max-Planck-Straße 1, 21502 Geesthacht, Germany; Claudio.Pistidda@hzg.de (C.P.); Jose.Bellostavoncolbe@hzg.de (J.B.v.C.); thomas.klassen@hzg.de (T.K.); Martin.Dornheim@hzg.de (M.D.)
3 Department of Metalphysics, Consejo Nacional de Investigaciones Científicas y Técnicas (CONICET) and Centro Atómico Bariloche, Av. Bustillo km 9500, San Carlos de Bariloche P.C. 8400, Argentina; viquiriglos@gmail.com
4 Instituto de Investigaciones Fisicoquímicas Teóricas y Aplicadas, INIFTA (CCT La Plata-CONICET, UNLP), Diagonal 113 y Calle 64, 1900 La Plata, Argentina; ramallolopez@gmail.com (J.M.R.-L.); melchanta@gmail.com (M.M.)
5 IFW Dresden, Helmholtzstr. 20, 01069 Dresden, Germany; T.Gemming@ifw-dresden.de
6 Institute of Materials Technology, Helmut Schmidt University, Holstenhofweg 85, 22043 Hamburg, Germany
* Correspondence: julianpuszkiel1979@gmail.com; Tel.: +49-0-4152-87-2601

Received: 11 October 2018; Accepted: 12 November 2018; Published: 19 November 2018

Abstract: Mg_2FeH_6 is regarded as potential hydrogen and thermochemical storage medium due to its high volumetric hydrogen (150 kg/m^3) and energy (0.49 kWh/L) densities. In this work, the mechanism of formation of Mg_2FeH_6 under equilibrium conditions is thoroughly investigated applying volumetric measurements, X-ray diffraction (XRD), X-ray absorption near edge structure (XANES), and the combination of scanning transmission electron microscopy (STEM) with energy-dispersive X-ray spectroscopy (EDS) and high-resolution transmission electron microscopy (HR-TEM). Starting from a 2Mg:Fe stoichiometric powder ratio, thorough characterizations of samples taken at different states upon hydrogenation under equilibrium conditions confirm that the formation mechanism of Mg_2FeH_6 occurs from elemental Mg and Fe by columnar nucleation of the complex hydride at boundaries of the Fe seeds. The formation of MgH_2 is enhanced by the presence of Fe. However, MgH_2 does not take part as intermediate for the formation of Mg_2FeH_6 and acts as solid-solid diffusion barrier which hinders the complete formation of Mg_2FeH_6. This work provides novel insight about the formation mechanism of Mg_2FeH_6.

Keywords: magnesium-iron complex hydride; equilibrium conditions; transmission electron microscopy; X-ray spectroscopy; hydrogen-energy storage

1. Introduction

The Mg–Fe–H system has interesting characteristics from the technological standpoint. Mg and Fe are cheap and broadly available metals. Under certain temperature and hydrogen pressure conditions, Mg_2FeH_6 is formed from a 2Mg:Fe elemental stoichiometric mixture. This complex hydride

has the highest hydrogen volumetric density (150 kg/m^3) among complex hydrides, relatively high hydrogen gravimetric density (5.5 wt % H_2), high reaction enthalpy (~90 kJ/mol H_2), and high volumetric (0.49 kWh/L) and gravimetric (0.55 kWh/kg) energy densities [1,2]. Owing to these characteristics, Mg_2FeH_6 has been investigated as thermochemical energy storage medium [1,3–7]. However, the synthesis of Mg_2FeH_6 is difficult due to the lack of a Mg_2Fe intermetallic [8]. Bogdanović et al. carried out a pioneering investigation via TEM-EDS observation about the formation mechanism of the Mg–Fe complex hydride. It was proposed that elemental Mg and Fe are the precursors for the formation of Mg_2FeH_6 under dynamic-cycling conditions. In addition, morphological analyses suggested that the formation mechanism occurs by the insertion of newly formed Mg_2FeH_6 at the phase boundary between Fe seeds and the growing Mg_2FeH_6 phase. This growth process provided a characteristic vermicular form for the initially formed Mg_2FeH_6 particles, which was kept even after hundreds of hydrogenation-dehydrogenation cycles [1]. Later investigations on the hydrogenation mechanism of Mg–Fe–H system, carried out under dynamic conditions, showed that the formation of Mg_2FeH_6 occurs via two consecutive reactions [9–12]. Mg_2FeH_6 was synthesized from stoichiometric mixture of 2Mg:Fe powder by reactive mechanical milling in hydrogen atmosphere via the intermediate formation of MgH_2, undergoing the simultaneous formation of MgH_2 and Mg_2FeH_6 [9]. Puszkiel et al. [11] found by in situ XRD experiments under 50 bar H_2 that MgH_2 is first formed at 215 °C from free Mg. Then, MgH_2 reacts with Fe to form Mg_2FeH_6 at 350 °C. The complete formation of Mg_2FeH_6 complex hydride is constrained at low temperature, due to kinetic restrictions related to solid-solid diffusion processes. The formation of MgH_2 from 2Mg:Fe is kinetically favored at temperatures around 200 °C. At higher temperatures, the solid-solid diffusion processes are enhanced, hence, Mg_2FeH_6 is formed from MgH_2 and Fe. It is also noted that the formation of Mg_2FeH_6 is not totally accomplished, since the solid–solid diffusion barriers between MgH_2 and Fe are not totally overcome [2,10,11]. Danaie et al. [12] also investigated the formation mechanism of Mg_2FeH_6 under dynamic conditions via STEM-EELS (scanning transmission electron microscopy-electron energy-loss spectroscopy) cooling down the sample in nitrogen. They found that, during the initial stage of the hydrogenation, MgH_2 is formed because the presence of Fe enhances the kinetic behavior. Then, Mg_2FeH_6 starts to nucleate by consuming the already-formed MgH_2 with a columnar morphology located between MgH_2 and Fe. This proposed formation mechanism agrees well with previous published works [9–12]. Furthermore, it was also pointed out that the columnar morphology coalesces when the material is kept at high temperature (400 °C) for long time.

In most of the cases, the synthesis of the Mg_2FeH_6 via different procedures such as thermal processes, mechanical milling, or their combinations, leads to yields between 25% and 90% and results in a MgH_2–Mg_2FeH_6 hydride mixture [1,3,9,13–39]. Studies on the thermodynamic properties of the MgH_2–Mg_2FeH_6 hydride mixture showed two different equilibrium pressures for the dehydrogenation process: the higher one belongs to MgH_2, while the lower one belongs to Mg_2FeH_6. However, upon hydrogenation from 2Mg:Fe stoichiometric mixture, the MgH_2–Mg_2FeH_6 hydride mixture presented one equilibrium pressure [1,20,21].

Herein, the formation mechanism of Mg_2FeH_6 under equilibrium conditions is, for the first time, investigated in detail to the best of our knowledge. For this purpose, pressure-composition isotherm (PCI) measurements are carried out in a Sieverts-type apparatus. Samples taken under equilibrium conditions at different hydrogen uptake stages are characterized by X-ray diffraction (XRD), X-ray absorption near edge structure (XANES), and the combination of scanning transmission electron microscopy (STEM) with energy-dispersive X-ray spectroscopy (EDS) and high-resolution transmission electron microscopy (HR-TEM). This work contributes to gaining more insight into the physicochemical properties of the Mg–Fe–H system as a potential thermochemical storage medium.

2. Materials and Methods

2.1. Preparation

2MgH_2:Fe stoichiometric powder mixture (MgH_2: Sigma Aldrich, purity >96.5% and Fe: Riedel-de Haën, purity >99.5%) was milled for 2 h under Ar atmosphere at 400 rpm in a P6-Fritsch mill device. A stainless steel (S.S.) milling chamber of 80 cm^3 and S.S. balls as grinding medium, with a ball to powder ratio of 40:1, were utilized.

2.2. Characterization

Hydrogenation and dehydrogenation pressure-composition isotherms (PCIs) were performed in a Sieverts-type device (in-house made, S.C. de Bariloche, Argentina) modified with flow controllers. The as-milled 2MgH_2:Fe was first dehydrogenated in non-isothermal conditions with a heating ramp of 10 °C/min under vacuum and then hydrogenation PCIs were measured with 2Mg:Fe as starting material. Hydrogenation-dehydrogenation PCIs at 400 °C were measured for different hydrogen capacities: 1 wt %, 2 wt %, 3 wt %, and complete PCI. Moreover, hydrogenation PCIs at 400 °C up to 1 wt %, 2 wt %, 3 wt % hydrogen capacities, and complete PCI, were measured and a sample at each point was taken for characterization.

Crystalline phase identification and microstructural characterization was done by X-ray diffraction (XRD) in a Philips PW 1710/01 (PANalytical, Worcestershire, UK) Instruments, with CuK_α radiation, λ = 1.5405 Å, graphite monochromator, 30 mA and 40 kV. The crystallite size was calculated with the Scherrer equation [40] using the following peaks: MgH_2 (2θ: 27.9°, (110)), Fe (2θ: 44.6°, (110)), Mg (2θ: 36.6°, (101)), and Mg_2FeH_6 (2θ: 24.1°, (111)).

X-ray absorption spectroscopy measurements (XAS) in the XANES (X-ray absorption near edge structure) and EXAFS (extended X-ray absorption fine structure) regions of hydrogenated samples under equilibrium conditions (1 wt %, 2 wt %, 3 wt %, and complete PCI) were carried out at the XAFS1 beamline of the Laboratório Nacional de Luz Síncrotron (LNLS), Campinas, Brazil, with a ring energy of 1.37 GeV, and a ring current of 250 mA [41]. The measurements were performed in transmission mode using a Si(111) channel cut monochromator around the Fe K-edge (7112 eV) in the range of energy from 6900 eV to 7900 eV at ambient temperature. The optimum amount of material for the measurements was calculated by the program XAFSMAS (version 2012/04, ALBA synchrotron, Barcelona, Spain) [42]. The samples were prepared by mixing them with boron nitride (25 mg, powder, purity: 98%; Sigma-Aldrich, St. Louis, Missouri, MO, USA,) in a mortar, and then pressing into pellets of 7 mm diameter inside a glove box. The pellets were put in a circular hole of an aluminum sample holder and sealed with Kapton tape (50 μm in thickness) to prevent the oxidation/hydrolysis of the samples. XAS data processing and fitting were performed by using the IFEFFIT software (version 1.2.11, University of Chicago, Chicago, IL, USA) package [43,44].

Scanning transmission electron microscopy (STEM) with energy-dispersive X-ray spectroscopy (EDS) and high-resolution transmission electron microscopy (HR-TEM) observations were done with a Tecnai F30 microscope (FEI Company, Hillsboro, OR, USA) with an information limit of 0.12 nm and Schottky field emission gun operating at 300 kV. Samples with different hydrogenation degrees (i.e., 1 wt %, 2 wt %, 3 wt %, and complete PCI) were prepared under equilibrium conditions at 400 °C. All the samples were prepared inside a glove box with controlled O_2 and H_2O atmosphere by dispersing the powders on lazy carbon and C film-supported grids with Cu frames. In order to avoid the short exposure time of the material and, at the time, introduce grids into the microscope column, the dispersed powder on the grid was covered with a special polymeric film which does not preclude the electron interactions with the sample. To identify the different Fe-rich zones, STEM observations using high-angle annular dark-field (HAADF) contrast and EDS analyses were performed first. Then, HR-TEM observations of the identified Fe zones were done. HR-TEM image processing was done with the following programs: Digital Micrograph (version GMS 2, Gatan, Pleasanton,

CA, USA), i-TEM (License no. A2382500, EMSIS GmbH, Münster, Germany), and JEMs (License no. IEb59yBDflUMh, CIME-EPFL, Lausanne, Switzerland).

Thermodynamic calculations were performed to evaluate the feasibility of the different reaction pathways for the formation mechanism of Mg_2FeH_6. These calculations were performed with the HSC Chemistry software 9.6.1 (Chemistry Software, Houston, TX, USA) [45]. Thermodynamic properties for Mg_2FeH_6 were added to the database for the calculations [46].

2.3. Handling

All handling was carried out in MBraun Unilab glove boxes (MBraun, Garching, Germany) with an oxygen- and moisture-controlled argon atmosphere (concentrations of <5 ppm of O_2 and H_2O) to prevent the oxidation of the samples.

3. Results

Figure 1 displays hydrogenation–dehydrogenation PCIs at 400 °C, and Figure 2 displays the XRD of the materials before and after the PCIs. The as-milled $2MgH_2$:Fe (Figure 2 (a)) was dehydrogenated, and then the 2Mg:Fe stoichiometric mixture was used as starting material for the PCIs measurements (ESI—Figure S1: A First non-isothermal dehydrogenation and B XRD after dehydrogenation). Complete PCI (Figure 1 (a)) leads to the formation of Mg_2FeH_6, MgH_2, and remnant Fe (Figure 2 (e)). The complete hydrogenation PCI (Figure 1 (a)) exhibits one plateau corresponding to the formation of both Mg_2FeH_6 and MgH_2. The complete dehydrogenation PCI (Figure 1 (b)) shows two distinct plateaus belonging to the decomposition of MgH_2 (higher equilibrium pressure) and Mg_2FeH_6 (lower equilibrium pressure) [1,20,21]. Dehydrogenation PCIs at different hydrogen capacities are shown in Figure 1 (c–e). For the dehydrogenation PCIs for different hydrogen capacities, hydrogenation PCIs have been previously done for the corresponding hydrogen capacities (ESI—Figure S2: Hydrogenation PCIs at 400 °C up to 1, 2, and 3 wt %). It is notable that the dehydrogenation PCIs from 1 wt % to 3 wt % (Figure 1 (c–e)) show two plateaus from the beginning of the hydrogenation process under equilibrium conditions.

Reflections from Mg_2FeH_6 and MgH_2, remnant Mg, and remnant Fe are observed in the XRD analyses of the samples partially hydrogenated under equilibrium conditions (Figure 2 (c–e), ESI—Figure S2). This result is in agreement with the two plateaus observed in the dehydrogenation PCIs (Figure 1 (c–e)). The crystallite sizes of Fe and MgH_2 after milling are 25 nm and 10 nm, respectively (Figure 2 (a)). During the hydrogenation process, i.e., 1 wt %, 2 wt %, and 3 wt %, the crystallite sizes of Fe and MgH_2 increase and keep around 30 nm and 40 nm, respectively (Figure 2 (b–d)). The crystallite size of free Mg upon hydrogenation is about 45 nm. Moreover, the formed Mg_2FeH_6 has a crystallite size of about 40 nm from 1 wt % to complete PCI (Figure 2 (b–e)).

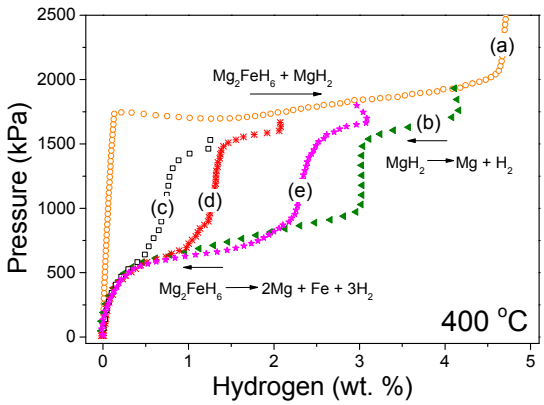

Figure 1. Pressure-composition isotherms (PCI) at 400 °C: (**a**) complete hydrogenation and (**b**) dehydrogenation, (**c**) dehydrogenation of a 1 wt % hydrogenated sample, (**d**) dehydrogenation of a 2 wt % hydrogenated sample, (**e**) dehydrogenation of a 3 wt % hydrogenated sample.

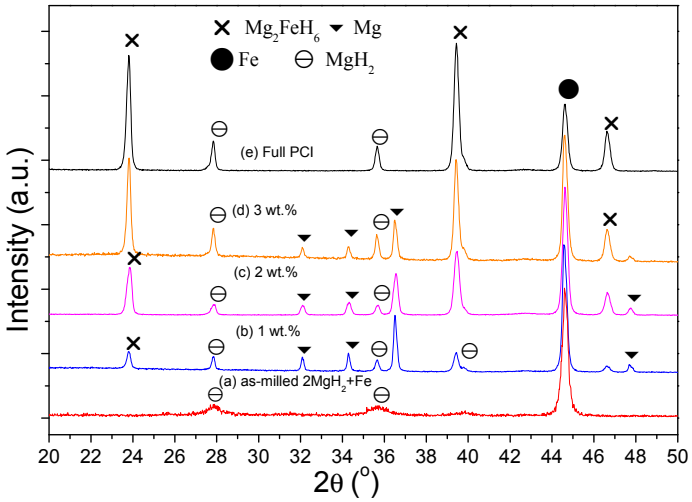

Figure 2. XRD: (**a**) $2MgH_2$:Fe after milling. Samples hydrogenated by PCIs at 400 °C up to (**b**) 1 wt % H_2, (**c**) 2 wt % H_2, (**d**) 3 wt % H_2, (**e**) complete hydrogenation. Note: the as-milled $2MgH_2$:Fe was first dehydrogenated to 2Mg:Fe and then hydrogenated via PCIs at 400 °C up to the indicated capacities.

In order to quantify the obtained amount of Mg_2FeH_6 during the hydrogenation process in equilibrium conditions, XANES measurements at the Fe K-edge were performed (ESI—Figure S3). The as-milled $2MgH_2$:Fe shows a XANES profile (ESI—Figure S3b) very similar to that of the metallic Fe (ESI—Figure S3a) with some slight differences. The other samples (ESI—Figure S3c–g) expose more notorious differences in the XANES spectra.

Fourier transforms of the as-milled $2MgH_2$:Fe and metallic Fe XANES spectra (ESI—Figure S4) show that all peaks in the metallic Fe are also present in as-milled $2MgH_2$:Fe. Comparison of the Fourier transforms (FT) of the EXAFS oscillations of the as-milled $2MgH_2$:Fe and metallic Fe (ESI—Figure S4) show that all peaks in the metallic Fe are also present in as-milled $2MgH_2$:Fe. It is noticed that the amplitudes of the Fourier transform of the as-milled $2MgH_2$:Fe are reduced. In order to quantitatively analyze these data, the main peaks have been isolated and fitted using standard procedures. Theoretical standards were generated by the FEFF program [44]. As an ab initio calculation, FEFF uses a list of atomic coordinates in a cluster and physical information about the system, such as type of absorbing atom and excited core-level for its calculation. In our case, the list of atomic coordinates has been simplified using ATOMS [47], which generates the required coordinates starting from a crystallographic description of the system. In the fitting, the bond distances, coordination numbers, Debye-Waller factors, and the parameter E_0 for each atomic pair have been allowed to vary independently. The reduction factor S_0^2 has been obtained from a Fe foil with a value of 0.72. The results obtained from the fit are shown in ESI—Table S1. The coordination numbers for the first two Fe–Fe shells in bulk metallic Fe are 8 and 6. A reduction in both average coordination numbers of the first two shells is found for the sample. This reduction can be a consequence of the nanometric size of the iron particles. In effect, as EXAFS probes all absorb atoms in the sample, those Fe atoms in the surface of a particle contribute with a lower coordination number that those in the bulk. The average coordination number is lower as the fraction of surface atoms is higher, that is, as the particle is smaller. Therefore, it is possible to ascribe the differences in the XANES spectra between metallic Fe and as-milled $2MgH_2$:Fe (ESI—Figure S4) to the contribution of these surface atoms, which will also show some slightly differences in their XANES spectra compared to atoms in the bulk. In consequence, for analyses of the XANES spectra of the rest of the samples, the spectrum of the $2MgH_2$:Fe sample will be used as that corresponding to nanometric metallic Fe particles. In the case of the XANES spectrum of the as-milled $2MgH_2$:Fe after several thermal processes (ESI—Figure S3g), it is different from the rest of the samples, and it is very similar to the one reported for Mg_2FeH_6 [48]. Results of the fitting of the EXAFS spectrum of this sample are shown in ESI (Figure S5, Table S2). It can be observed that the

first two shells surrounding Fe atoms are very similar to those in the hydride Mg_2FeH_6 in which Fe atoms have 8 hydrogen atoms at 1.557 Å and 8 Mg atoms at 2.787 Å [13].

The XANES spectra of samples obtained at different stages of the hydrogenation PCI at 400 °C (ESI—Figure S3c–f) have been analyzed by linear combination fitting (LCF) of the data with reference compounds using ATHENA program (version 0.8.056, University of Chicago, Chicago, IL, USA) [43]. It is important to point out that two reference spectra are enough to reproduce all sample spectra: nanometric metallic Fe particles (spectrum of the as-milled $2MgH_2$:Fe, ESI—Figure S3b) and Mg_2FeH_6 (spectrum of the as-milled $2MgH_2$:Fe after several thermal processes, ESI—Figure S3g). Figure 3 shows the results of the LCF of all samples. It is found that after the absorption of 1 wt % of H_2, 12% of Mg_2FeH_6 is formed, and its quantity rises as the hydrogen capacity increases, i.e., 24% and 39% for 2 wt % H_2, 3 wt % H_2, respectively. The remnant Fe atoms remain as nanometric metallic particles. When the PCI is completed, the percentage of Mg_2FeH_6 reaches a maximum of 44%. Furthermore, there is an apparent broadening of the peaks produced by the decrease of the quantity of the metallic Fe nanoparticles present in the sample with the increase of the H_2 amount (ESI Figure S3). The XANES spectra are the result of the convolution of the two Fe species present in the samples, i.e., Fe and Mg_2FeH_6. This effect is clearly seen on Figure 3, where the linear combination fitting of the XANES spectra is shown, as well as the proportion of each of the two components used for the fitting.

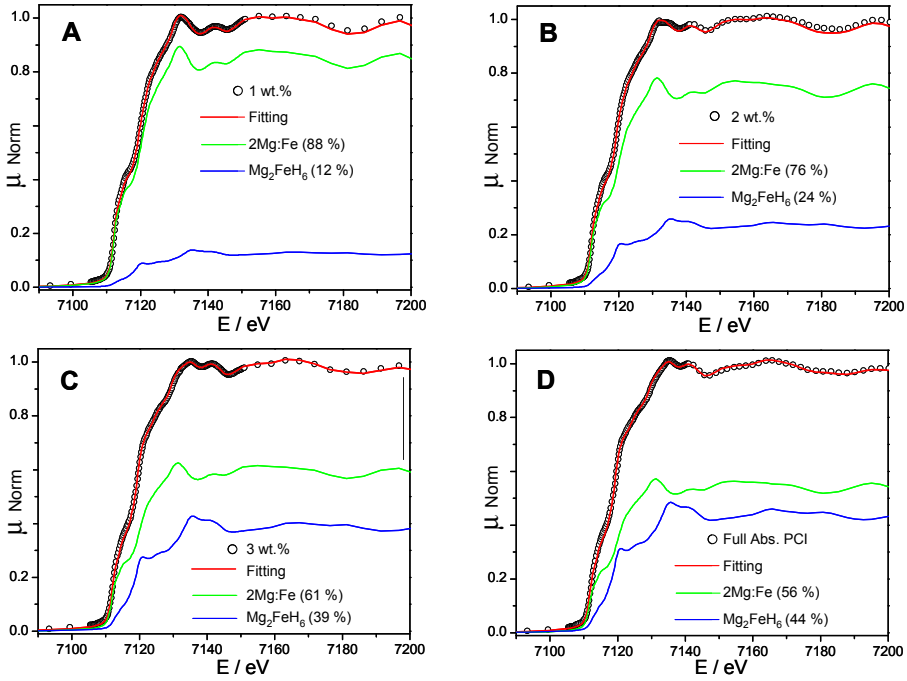

Figure 3. Linear combination fitting of XANES spectra. Absorption PCI at 400 °C from dehydrogenated as-milled $2MgH_2$:Fe up to: (**A**) 1 wt % H_2, (**B**) 2 wt % H_2, (**C**) 3 wt % H_2, (**D**) complete hydrogenation PCI.

Calculations of the percentages of the hydride phases from the dehydrogenation PCIs (Figure 1 (b–e)) have been also carried out. These calculations have been done taking into account the hydrogen capacities released in each dehydrogenation plateau, and the 2Mg:Fe stoichiometric mixture, as explained in a previous work [21]. The calculated relative amounts are shown in Table 1. In parentheses are shown the amounts of Mg_2FeH_6 obtained from the XANES analysis. Despite the fact that, in some cases, the relative amounts of Mg_2FeH_6 calculated from the PCIs are slightly higher than the ones obtained from XANES spectra fitting, both results are in good agreement.

Materials after hydrogenation PCIs at 400 °C (Figure 1) at different stages were characterized by combined scanning transmission electron microscopy (STEM) with energy-dispersive X-ray spectroscopy (EDS) and high-resolution transmission electron microscopy (HR-TEM). Figure 4 shows

STEM observations and EDS measurements after 1 wt % and 3 wt % hydrogenation PCIs at 400 °C. It is possible to observe that the bright regions belong to Fe-rich zones, and the dark regions correspond to Mg-rich zones. In all the bright regions, there are considerable amounts of Mg. In addition, bright particles present a kind of elongated and columnar shape, and are imbedded in dark matrices composed of Mg-rich zones. The presence of Cu in the EDS spectra comes from the Cu frames of the carbon supported grids used as sample holders.

Table 1. Relative amounts of phases calculated from PCIs for the different hydrogenation stage of 2Mg:Fe and starting 2Mg:Fe composition. The amounts of Mg_2FeH_6 obtained from the XANES analysis are indicated in parentheses.

Hydrogenation State	Amounts of Phases (wt %)			
	Mg	**Fe**	**MgH_2**	**Mg_2FeH_6**
2Mg:Fe	46	54	-	-
1 wt %	34	46	6	14 (12)
2 wt %	26	40	10	24 (24)
3 wt %	18	31	10	41 (39)
Complete PCI	4	28	22	46 (44)

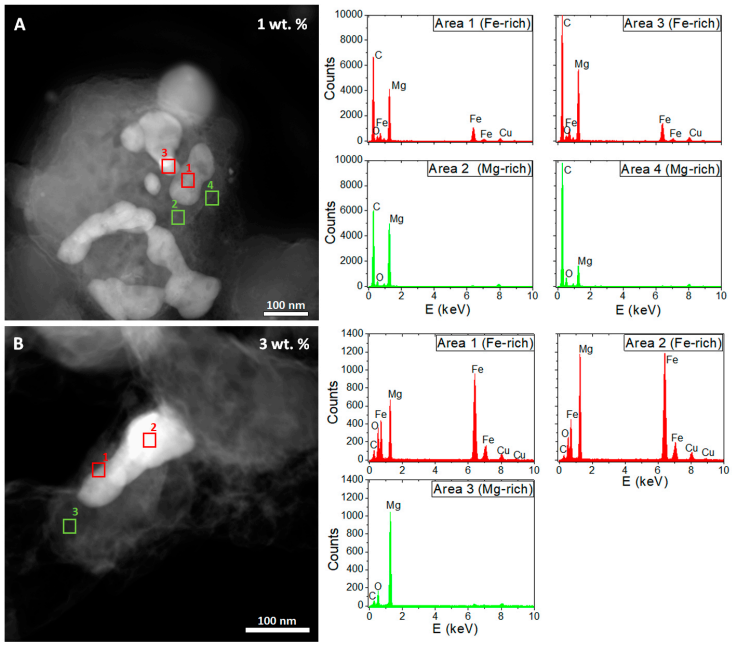

Figure 4. STEM-EDS results for samples after absorption PCI at 400 °C from dehydrogenated as-milled $2MgH_2$:Fe up to (**A**) 1 wt % H_2, (**B**) 3 wt % H_2.

Figure 5 shows STEM observations, EDS analyses, and HR-TEM images along with FFT analyses and their simulation patterns for the different stages of the hydrogenation under equilibrium conditions (Figure 1. PCI at 400 °C: 1 wt %, 2 wt %, and 3 wt %). Reduced region of the STEM images are shown in Figure 4 for 1 wt % and 3 wt %, and additional EDS analyses are presented in Figure 5. HR-TEM photos performed at the interfaces between the Fe-rich and Mg-rich regions evidence a common feature (HR-TEM images: Figure 5A–C). At the Fe-rich zone (bright region in STEM, dark region in HR-TEM), FFT analyses and structure simulations show Mg_2FeH_6 patterns and Mg + Mg_2FeH_6 overlapped patterns. At the Mg-rich zones (dark region in STEM, bright region in HR-TEM), FFT analyses and structure simulations exhibit mostly MgH_2 patterns and Mg + MgH_2 overlapped patterns. In the sample hydrogenated up to 3 wt %, the Fe-rich zone (Figure 5C HR-TEM2b) is surrounded by a large number of MgH_2, related with the hydrogenation stage near the saturation of the material.

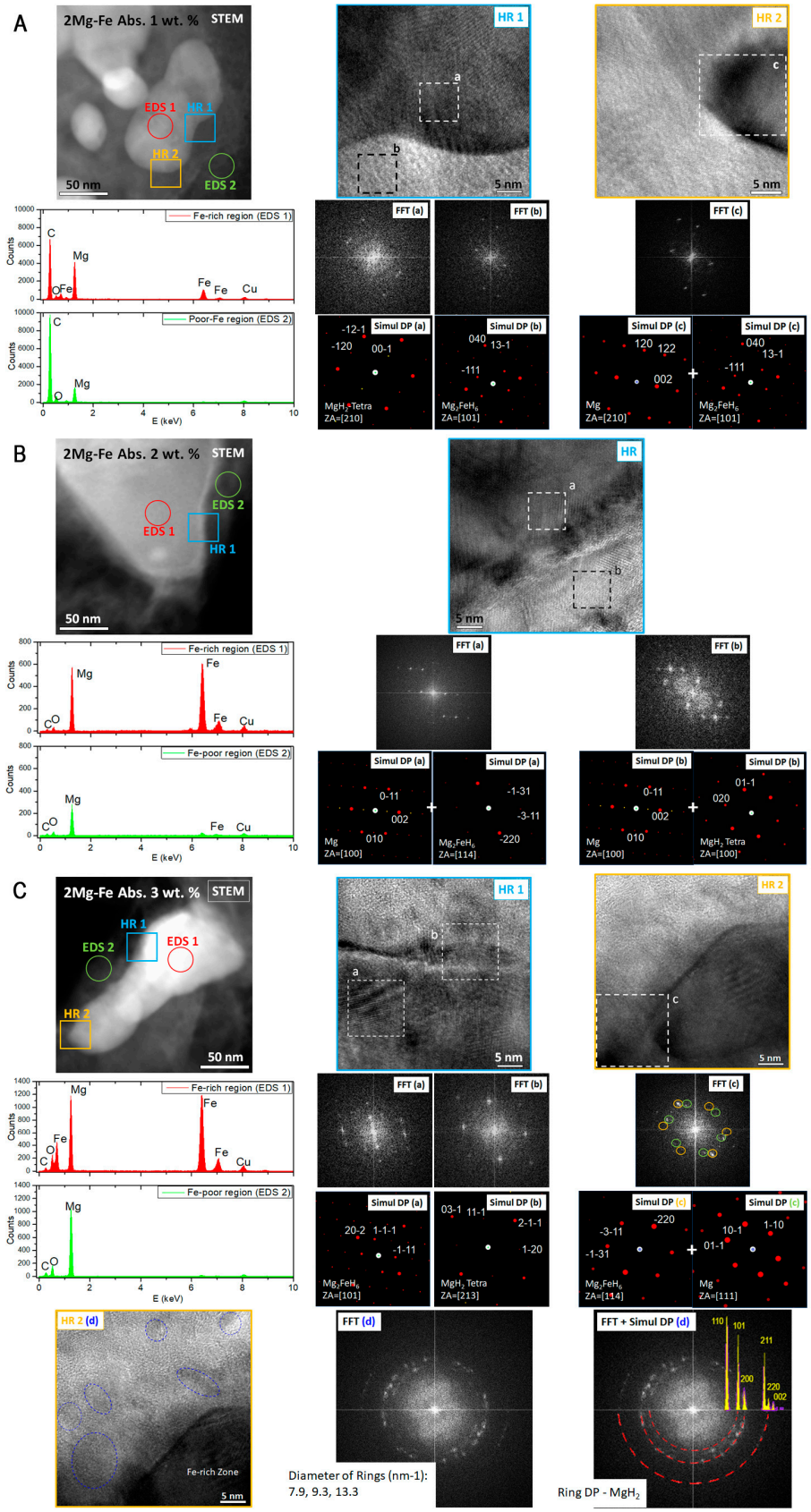

Figure 5. STEM-EDS, HR-TEM, FFT, and simulations for samples after absorption PCI at 400 °C from dehydrogenated as-milled $2MgH_2$:Fe up to (**A**) 1 wt % H_2, (**B**) 2 wt % H_2, **C** 3 wt % H_2. Width of FFT and simulation images: 18 nm^{-1}.

4. Discussion

In this work, from the beginning of the hydrogenation PCI (Figure 1a), the hydride phases Mg_2FeH_6 and MgH_2 are present. This fact can be observed in the dehydrogenation PCIs curves (Figure 1 (c–e)), XRD analyses (Figure 2 (b–d)), and the phase amounts calculated from the PCIs and XANES spectra fitting. Thus, the question arises whether the mechanism of formation of Mg_2FeH_6 occurs from elemental Mg and Fe, from MgH_2 and Fe, or from mixed reactions.

At the beginning of PCI at 400 °C, about 14 wt % of Mg_2FeH_6 and a small amount of MgH_2 of roughly 6 wt % (Figure 1 (c)) are formed (Table 1). TEM investigations (Figures 4 and 5 STEM) show that, for the stage at 1 wt %, the Mg_2FeH_6 starts to nucleate in the Fe-rich zones in columnar and elongated shapes, and sizes ranging 50 nm to 200 nm. The analyses of the diffraction patterns (Figure 5A HR-TEM-FFT) at the interfaces evidence overlapped Mg and Mg_2FeH_6 in the Fe-rich zones. In the surroundings of Fe-rich zones, STEM-EDS and FFT-simulation analysis indicate the presence of Mg-rich zones with diffraction patterns belonging to Mg and MgH_2. It is possible to infer that the presence of Fe catalyzes the formation of MgH_2 in agreement with a previous work [12]. As the hydrogenation PCI proceeds, at 2 wt % and 3 wt % of hydrogen capacity (Figure 1 (d,e)), the amount of Mg_2FeH_6 increases about twofold up to 24 wt % and 41 wt % (Table 1), respectively, while MgH_2 just reaches 10 wt % for 2 and 3 wt % of hydrogen capacity. At theses stages, it is clear that MgH_2 is neither formed nor consumed. Moreover, TEM investigations (Figure 5B,C) also show overlapped patterns of Mg_2FeH_6 and Mg. Interestingly, the elongated shapes made of Fe-rich particles is kept. Moreover, the particle size of the Fe rich zone and the crystallite size of Mg_2FeH_6 and MgH_2 remain almost constant upon all the PCI hydrogenation process.

Finally, after complete PCI, the formation of Mg_2FeH_6 is not completely achieved. The amount of formed Mg_2FeH_6 increases just about 5 wt %, while the amount of MgH_2 notably increases again to 22 wt % (Table 1). MgH_2 is formed around the Fe-rich zones, as shown for the sample at 3 wt % of hydrogen capacity (Figure 5C HR-TEM2b).

Standard free energy calculations for the different routes of formation of Mg_2FeH_6 are shown as follows:

$$2Mg_{(s)} + Fe_{(s)} + 3H_{2(g)} \rightarrow Mg_2FeH_{6(s)}\ \Delta G^\circ = -30.4\ \text{kJ/mol}, \quad (1)$$

$$2MgH_{2(s)} + Fe_{(s)} + H_{2(g)} \rightarrow Mg_2FeH_{6(s)}\ \Delta G^\circ = 42.5\ \text{kJ/mol}, \quad (2)$$

$$MgH_{2(s)} + Mg_{(s)} + Fe_{(s)} + 2H_{2(g)} \rightarrow Mg_2FeH_{6(s)}\ \Delta G^\circ = 5.9\ \text{kJ/mol}. \quad (3)$$

The formation of Mg_2FeH_6 from elemental Mg and Fe is the most thermodynamically favorable reaction. Ab initio calculations, based on density functional theory (DFT) about the formation mechanism of Mg_2FeH_6, have also reported reaction (1) as the optimum route from the thermodynamic point of view, regardless of any kinetic constraints [49].

Considering all the experimental evidence (Figures 1–5 and Table 1) and based on the calculations of the standard free energy for the possible formation reactions of Mg_2FeH_6, it is possible to propose a reaction mechanism for Mg_2FeH_6 formation under equilibrium conditions. Mg_2FeH_6 nucleates from elemental Fe and Mg in a columnar form at the phase boundary between Fe seeds and the growing Mg_2FeH_6 phase, in agreement with the mechanism in dynamic conditions proposed by Bogdanović et al. [1]. Upon hydrogenation PCI, the formation of MgH_2 is thermodynamically feasible, since the equilibrium pressure at 400 °C for the Mg–H system is similar to the one for Mg–Fe–H system, and the MgH_2 formation is enhanced by the presence of Fe [11,12,20,21]. However, MgH_2 does not take part as intermediate for the formation of Mg_2FeH_6, based on the relative amounts of phases (Table 1) and TEM investigations (Figure 5). At the end of the hydrogenation PCI, the partial formation of Mg_2FeH_6 can be attributed to the presence of MgH_2 around Fe-rich particles (Figures 4 and 5) acting as a solid–solid diffusion barrier.

5. Conclusions

The formation mechanism of Mg_2FeH_6 complex hydride under equilibrium conditions was investigated by the volumetric technique (PCI measurements at 400 °C), and microstructural, nanostructural, and chemical characterization techniques: XRD, STEM-EDS combined with HR-TEM and XANES, respectively. Based on analyses of experimental results supported by standard free energy calculations for the possible reaction pathway, the formation mechanism of Mg_2FeH_6 under equilibrium conditions is proposed here. From the beginning of the hydrogenation PCI, Mg_2FeH_6 and MgH_2 are present. On the one hand, Mg_2FeH_6 nucleates from elemental Fe and Mg in a columnar form at the phase boundary between Fe seeds and the growing Mg_2FeH_6 phase. On the other hand, the formation of MgH_2 is enhanced by the presence of Fe, but it does not take part as intermediate in the formation of Mg_2FeH_6. However, at the end of the hydrogenation PCI, the partial formation of Mg_2FeH_6 can be attributed to the presence of MgH_2 around Fe-rich particles acting as a solid-solid diffusion barrier. This investigation provided novel insight about the formation mechanism of Mg_2FeH_6, useful for further improvement of this Mg-based complex hydride for its potential application as a thermochemical storage medium.

Supplementary Materials: The following are available online at http://www.mdpi.com/2075-4701/8/11/967/s1, Figure S1. A First non-isothermal dehydrogenation for the as-milled $2MgH_2$–Fe at a heating ramp of 10 °C/min and 20 kPa and B XRD after dehydrogenation, Figure S2. Hydrogenation PCIs at 400 °C for 2Mg:Fe (as-milled $2MgH_2$–Fe dehydrogenated as indicated in Figure S1) up to: A 1 wt %, B 2 wt % and C 3 wt % of hydrogen capacity, Figure S3. XANES spectra at the Fe K-edge of (a) metallic Fe, (b) as-milled $2MgH_2$ + Fe, samples hydrogenated in equilibrium conditions at 400 °C up to: (c) 1 wt % H_2, (d) 2 wt % H_2, (e) 3 wt % H_2, (f) Complete PCI at 400 °C and (g) Mg_2FeH_6 obtained after several thermal processes at high temperature and under high pressure from as-milled $2MgH_2$+Fe, Figure S4. Comparison of the amplitude of the Fourier Transforms of the EXAFS oscillations of metallic Fe (black) and as-milled $2MgH_2$ + Fe (red). Table S1. Results of the EXAFS fit for as-milled $2MgH_2$ + Fe, Figure S5. Fitting of the Fourier Transform of the EXAFS signal of as-milled $2MgH_2$ + Fe after several thermal processes (corresponding XANES spectrum Figure S3g). Black circles: experimental data. Solid line: fitting function, Table S2. Results of the EXAFS fit for as-milled $2MgH_2$ + Fe after several thermal processes (XANES spectrum Figure S2g).

Author Contributions: J.P. conceived the design of the structure of the work, wrote the paper and contribute with the experiments. M.V.C.R. performed the STEM-TEM observation and analyses of the results and contributed with the interpretation and writing. F.G. and P.A.L. contributed with the conception, experiments, writing and corrections of the manuscript. J.M.R.-L. and M.M. performed the XAS measurements and contributed with the writing and corrections of the manuscript. C.P., M.D. and T.G. contributed with the discussion and corrections. J.B.v.C. and T.K. contributed with the corrections of the manuscripts.

Funding: This research received no external funding.

Acknowledgments: The authors thank CONICET (Consejo Nacional de Invetigaciones Científicas y Técnicas), ANPCyT (Agencia Nacional de Promoción Científica y Tecnológica)-PICT 2015 1865 and PICT 2015 2285, CNEA (Comisión Nacional de Energía Atómica), Instituto Balseiro (UNCuyo) and Universidad Nacional de La Plata (UNLP, Project 11/X790) for financial support to carry out this work. Partial support by Laboratório Nacional de Luz Síncrotron (LNLS), Campinas, Brazil (proposal XAFS1-15239) is acknowledged. The Department of Nanotechnology of the Helmholtz Zentrum Geesthacht, Germany is acknowledged for the financial support and discussion.

Conflicts of Interest: The authors declare no conflict of interest.

References

1. Bogdanović, B.; Reiser, A.; Schlichte, K.; Spliethoff, B.; Tesche, B. Thermodynamics and dynamics of the Mg–Fe–H system and its potential for thermochemical thermal energy storage. *J. Alloy. Compd.* **2002**, *345*, 77–89. [CrossRef]
2. Puszkiel, J.; Andrade-Gamboa, J.; Gennari, F.C. Recent Progress in Mg–Co–H and Mg–Fe–H Systems for Hydrogen Energy Storage Applications. In *Emerging Materials for Energy Conversion and Storage*, 1st ed.; Cheong, K.Y., Impellizzeri, G., Fraga, M., Eds.; Elsevier: Cambridge, UK, 2018; pp. 393–428.
3. Reiser, A.; Bogdanović, B. The application of Mg-based metal-hydrides as heat energy storage systems. *Int. J. Hydrogen Energy* **2000**, *25*, 425–430. [CrossRef]

4. Crivello, J.-C.; Denys, R.V.; Dornheim, M.; Felderhoff, M.; Grant, D.M.; Huot, J.; Jensen, T.R.; de Jongh, P.; Latroche, M.; Walker, G.S.; et al. Mg-based compounds for hydrogen and energy storage. *Appl. Phys. A* **2016**, *122*, 1–17. [CrossRef]
5. Felderhoff, M.; Bogdanović, B. High temperature metal hydrides as heat storage materials for solar and related applications. *Int. J. Mol. Sci.* **2009**, *10*, 325–344. [CrossRef] [PubMed]
6. Urbanczyk, R.; Meggouh, M.; Moury, R.; Peinecke, K.; Peil, S.; Felderhoff, M. Demonstration of Mg_2FeH_6 as heat storage material at temperatures up to 550 °C. *Appl. Phys. A* **2016**, *122*, 315–320. [CrossRef]
7. Urbanczyk, R.; Peinecke, K.; Peil, S.; Felderhoff, M. Development of a heat storage demonstration unit on the basis of Mg_2FeH_6 as heat storage material and molten salt as heat transfer media. *Int. J. Hydrogen Energy* **2017**, *42*, 13818–13826. [CrossRef]
8. Massalski, T. *Binary Alloy Phase Diagram*, 2nd ed.; ASM International: Metals Park, OH, USA, 1990; pp. 1722–1723.
9. Gennari, F.C.; Castro, F.J.; Andrade Gamboa, J.J. Synthesis of Mg_2FeH_6 by reactive mechanical alloying: Formation and decomposition properties. *J. Alloy. Compd.* **2002**, *339*, 261–267. [CrossRef]
10. Polanski, M.; Nielsen, T.K.; Cerenius, Y.; Bystrzycki, J.; Jensen, T.R. Synthesis and decomposition mechanisms of Mg_2FeH_6 studied by in-situ synchrotron X-ray diffraction and high-pressure DSC. *Int. J. Hydrogen Energy* **2010**, *35*, 3578–3582. [CrossRef]
11. Puszkiel, J.A.; Gennari, F.; Arneodo Larochette, P.; Karimi, F.; Pistidda, C.; Gosalawit-Utke, R.; Jepsen, J.; Jensen, T.R.; Gundlach, C.; von Colbe, J.B.; et al. Sorption behavior of the MgH_2-Mg_2FeH_6 hydride storage system synthesized by mechanical milling followed by sintering. *Int. J. Hydrogen Energy* **2013**, *38*, 14618–14630. [CrossRef]
12. Danaie, M.; Asselli, A.A.C.; Huot, J.; Botton, G.A. Formation of the ternary complex hydride Mg_2FeH_6 from magnesium hydride (β-MgH_2) and iron: An electron microscopy and energy-loss spectroscopy study. *J. Phys. Chem. C* **2012**, *116*, 25701–25714. [CrossRef]
13. Didisheim, J.J.; Zolliker, P.; Yvon, K.; Fischer, P.; Schefer, J.; Gubelmann, M. Dimagnesium iron (II) hydride, Mg_2FeH_6, containing octahedral $[FeH_6]^{4-}$ anions. *Inorg. Chem.* **1984**, *23*, 1953–1957. [CrossRef]
14. Selvam, P.; Yvon, K. Synthesis of Mg_2FeH_6, Mg_2CoH_5 and Mg_2NiH_4 by high-pressure sintering of the elements. *Int. J. Hydrogen Energy* **1991**, *16*, 615–617. [CrossRef]
15. Huot, J.; Hayakawa, H.; Akiba, E. Preparation of the hydrides Mg_2FeH_6 and Mg_2CoH_5 by mechanical alloying followed by sintering. *J. Alloy. Compd.* **1997**, *248*, 164–167. [CrossRef]
16. Konstanchuk, I.G.; Ivanov, E.Y.; Pezat, M.; Darriet, B.; Boldyrev, V.V.; Hagenmuller, P. The hydriding properties of a mechanical alloy with composition Mg-25%Fe. *J. Less Common Met.* **1987**, *131*, 181–189. [CrossRef]
17. Retuerto, M.; Sánchez-Benítez, J.; Rodríguez-Cañas, E.; Serafini, D.; Alonso, J.A. High-pressure synthesis of Mg_2FeH_6 complex hydride. *Int. J. Hydrogen Energy* **2010**, *35*, 7835–7841. [CrossRef]
18. Niaz, N.A.; Ahmad, I.; Khalid, N.R.; Ahmed, E.; Abbas, S.M.; Jabeen, N. Preparation of Mg_2FeH_6: Nanoparticles for hydrogen storage properties. *J. Nanomater.* **2013**, 1–7. [CrossRef]
19. Ivanov, E.; Konstanchuk, I.; Stepanov, A.; Boldyrev, V. Magnesium mechanical alloys for hydrogen storage. *J. Less Common Met.* **1987**, *131*, 25–29. [CrossRef]
20. Puszkiel, J.A.; Arneodo Larochette, P.; Gennari, F.C. Thermodynamic and kinetic studies of Mg-Fe-H after mechanical milling followed by sinterin. *J. Alloy. Compd.* **2008**, *463*, 134–142. [CrossRef]
21. Puszkiel, J.A.; Arneodo Larochette, P.; Gennari, F.C. Thermodynamic and kinetic characterization of the synthesized Mg_2FeH_6–MgH_2 hydrides mixture. *Int. J. Hydrogen Energy* **2008**, *33*, 3555–3560. [CrossRef]
22. Riktor, M.D.; Deledda, S.; Herrich, M.; Gutfleisch, O.; Fjellvåg, H.; Hauback, B.C. Hydride formation in ball-milled and cryomilled Mg-Fe powder mixtures. *Mater. Sci. Eng. B* **2009**, *158*, 19–25. [CrossRef]
23. Polanski, M.; Płociński, T.; Kunce, I.; Bystrzycki, J. Dynamic synthesis of ternary Mg_2FeH_6. *Int. J. Hydrogen Energy* **2010**, *35*, 1257–1266. [CrossRef]
24. Polanski, M.; Witek, K.; Nielsen, T.K.; Jaroszewicz, L.; Bystrzycki, J. The influence of the milling time on the yield of Mg_2FeH_6 from a two-step synthesis conducted in a custom-made reactor. *Int. J. Hydrogen Energy* **2013**, *38*, 2785–2789. [CrossRef]
25. Zhang, J.; Cuevas, F.; Zaïdi, W.; Bonnet, J.P.; Aymard, L.; Bobet, J.L.; Latroche, M. Highlighting of a single reaction path during reactive ball milling of Mg and TM by quantitative H_2 gas sorption analysis to form ternary complex hydrides (TM = Fe, Co, Ni). *J. Phys. Chem. C* **2011**, *115*, 4971–4979. [CrossRef]

26. Huot, J.; Boily, S.; Akiba, E.; Schulz, R. Direct synthesis of Mg_2FeH_6 by mechanical alloying. *J. Alloy. Compd.* **1998**, *280*, 306–309. [CrossRef]
27. Castro, F.J.; Gennari, F.C. Effect of the nature of the starting materials on the formation of Mg_2FeH_6. *J. Alloy. Compd.* **2004**, *375*, 292–296. [CrossRef]
28. Herrich, M.; Ismail, N.; Lyubina, J.; Handstein, A.; Pratt, A.; Gutfleisch, O. Synthesis and decomposition of Mg_2FeH_6 prepared by reactive milling. *Mater. Sci. Eng. B* **2004**, *108*, 28–32. [CrossRef]
29. Varin, R.A.; Li, S.; Calka, A.; Wexler, D. Formation and environmental stability of nanocrystalline and amorphous hydrides in the 2Mg-Fe mixture processed by controlled reactive mechanical alloying (CRMA). *J. Alloy. Compd.* **2004**, *373*, 270–286. [CrossRef]
30. Li, S.; Varin, R.A.; Morozova, O.; Khomenko, T. Controlled mechano-chemical synthesis of nanostructured ternary complex hydride Mg_2FeH_6 under low-energy impact mode with and without pre-milling. *J. Alloy. Compd.* **2004**, *384*, 231–248. [CrossRef]
31. Varin, R.A.; Li, S.; Wronski, Z.; Morozova, O.; Khomenko, T. The effect of sequential and continuous high-energy impact mode on the mechano-chemical synthesis of nanostructured complex hydride Mg_2FeH_6. *J. Alloy. Compd.* **2005**, *390*, 282–296. [CrossRef]
32. Zhou, D.W.; Li, S.L.; Varin, R.A.; Peng, P.; Liu, J.S.; Yang, F. Mechanical alloying and electronic simulations of 2Mg-Fe mixture powders for hydrogen storage. *Mater. Sci. Eng. A* **2006**, *427*, 306–315. [CrossRef]
33. Wronski, Z.; Varin, R.A.; Chiu, C.; Czujko, T.; Calka, A. Mechanochemical synthesis of nanostructured chemical hydrides in hydrogen alloying mills. *J. Alloy. Compd.* **2007**, *434*, 743–746. [CrossRef]
34. Varin, R.A.; Czujko, T.; Wronski, Z.S. *Nanomaterials for Solid State Hydrogen Storage*, 1st ed.; Springer: New York, NY, USA, 2008; pp. 1–325.
35. Sai Raman, S.S.; Davidson, D.J.; Bobet, J.-L.; Srivastava, O.N. Investigations on the synthesis, structural and microstructural characterization of Mg based K_2PtCl_6-type (Mg_2FeH_6) hydrogen storage material prepared by mechanical alloying. *J. Alloy. Compd.* **2002**, *333*, 282–290. [CrossRef]
36. Wang, Y.; Cheng, F.; Li, C.; Tao, Z.; Chen, J. Preparation and characterization of nanocrystalline Mg_2FeH_6. *J. Alloy. Compd.* **2010**, *508*, 554–558. [CrossRef]
37. Asselli, A.C.C.; Leiva, D.R.; Jorge, A.M.; Ishikawa, T.T.; Botta, W.J. Synthesis and hydrogen sorption properties of MgH_2-Mg_2FeH_6 nanocomposites prepared by reactive milling. *J. Alloy. Compd.* **2012**, *536*, S250–S254. [CrossRef]
38. Nyamsi, S.N.; Yartys, V.; Lototskyy, M. Synthesis of Mg_2FeH_6 Assisted by Heat Treatment of Starting Materials. In Proceedings of the 1st Africa Energy Materials Conference, Pretoria, South Africa, 28–31 March 2017.
39. Jung, J.Y.; Fadonougbo, J.O.; Suh, J.-Y.; Lee, Y.-S.; Huh, Y.-J.; Cho, Y.W. Synthesis of Mg_2FeH_6 by hydrogenation of Mg/Fe powder mixture prepared by cold roll milling in air: Effects of microstructure and oxygen distribution. *Int. J. Hydrogen Energy* **2018**, *43*, 16758–16765. [CrossRef]
40. Alexander, L.; Klug, P.H. Determination of crystallite size with the x-ray spectrometer. *J. Appl. Phys.* **2004**, *21*, 137. [CrossRef]
41. Laboratorio Nacional de Luz Síncrotron (LNLS). Available online: http://www.lnls.br/28 (accessed on 11 October 2018).
42. XAFSmass, Freeware. Available online: www.cells.es/Beamlines/CLAESS/software/xafsmass.html (accessed on 11 October 2018).
43. Ravel, B.; Newville, M. ATHENA, ARTEMIS, HEPHAESTUS: Data analysis for X-ray absorption spectroscopy using IFEFFIT. *J. Synchrotron Radiat.* **2005**, *12*, 537–541. [CrossRef] [PubMed]
44. Zabinsky, S.I.; Rehr, J.J.; Ankudinov, A.; Albers, R.C.; Eller, M.J. Multiple-scattering calculations of x-ray-absorption spectra. *J. Phys. Rev. B* **1995**, *52*, 2995–3009. [CrossRef]
45. Roine, A. *Outokumpu HSC Chemistry for Windows*; Outokumpu Research Oy: Pori, Finland, 2009.
46. Zhou, H.L.; Yu, Y.; Zhang, H.F.; Gao, T. Structural, vibrational and thermodynamic properties of Mg2FeH6 complex hydride. *Eur. Phys. J. B* **2011**, *79*, 283–288. [CrossRef]
47. Ravel, B. ATOMS: Crystallography for the X-ray absorption spectroscopist. *J. Synchrotron Radiat.* **2001**, *8*, 314–316. [CrossRef] [PubMed]

48. Zhang, J.; Zaïdi, W.; Paul-Boncour, V.; Provost, K.; Michalowicz, A.; Cuevas, F.; Latroche, M.; Belin, S.; Bonnet, J.-P.; Aymard, L. XAS investigations on nanocrystalline Mg_2FeH_6 used as a negative electrode of Li-ion batteries. *J. Mater. Chem. A* **2013**, *1*, 4706–4717. [CrossRef]
49. Zareii, S.M.; Sarhaddi, R. Structural, electronic properties and heat of formation of Mg_2FeH_6 complex hydride: An ab initio study. *Phys. Scr.* **2012**, *86*, 015701. [CrossRef]